Available online at www.sciencedirect.com
SCIENCE DIRECT®
Journal of Sound and Vibration 296 (2006) 447–460
JOURNAL OF SOUND AND VIBRATION
www.elsevier.com/locate/jsvi

An experimental investigation of unsteady surface pressure on an airfoil in turbulence—Part 2: Sources and prediction of mean loading effects

Patrick F. Mish*, William J. Devenport

Virginia Tech, Aerospace and Ocean Engineering Department, 215 Randolph Hall, Blacksburg, VA 24060, USA

Received 30 April 2003; received in revised form 6 July 2005; accepted 22 August 2005
Available online 9 June 2006

Abstract

An experimental investigation into the response of an airfoil in turbulence was undertaken and the results are presented in a two part series of papers. The effects of mean loading on the airfoil response are investigated in Part 1 with the likely origins discussed in this paper (Part 2). Unsteady pressure measurements were made on the surface of a NACA 0015 airfoil immersed in grid turbulence ($\lambda/c = 13\%$) for angles of attack $\alpha = 0$–20°. This paper (Part 2) presents the causes of the low-frequency reduction and high-frequency increase observed in measured lift and pressure spectral levels. Scaling lift spectra on the mean lift reveals the increase in lift spectral level for reduced frequencies greater than 10 is closely related to the airfoils mean pressure field. Based on analysis of the chordwise and spanwise pressure correlation length scale, the reduction in lift spectral level at low reduced frequency appears to result from distortion of the inflow by the mean velocity field. A possible model is developed that accurately predicts mean loading effects on lift spectra. This model uses a circular cylinder fit to the airfoil to compute effects of distortion on the inflow turbulence. The distorted inflow velocity spectrum is then used with Amiet's theory to predict the unsteady loading. This model successfully captures the reduction observed in measured lift spectra at low reduced frequencies. Furthermore, it is shown that the angle of attack effects arising from inflow distortion are significant only when the relative scale of the inflow turbulence to airfoil chord is sufficiently small ($\lambda/c = 13\%$ for present experiment).

1. Introduction

An airfoil moving through a turbulent stream experiences surface pressure fluctuations that can produce vibration and radiate broadband noise. Throughout the past 60 years many researchers have worked on mathematical models of turbulence–airfoil interaction with nearly as many models developed as years spent working on the problem. The large number of models arises as a result of the complexity of the problem and the desire for efficient solutions that can be implemented in early design of aircraft and turbo-machinery. However, as mathematical representations of turbulence–airfoil interaction have flourished, surprisingly few experiments have been performed to allow for systematic verification of these models.

*Corresponding author. Tel.: +1 410 279 8772.
E-mail address: pmish@vt.edu (P.F. Mish).

0022-460X/$ - see front matter © 2005 Published by Elsevier Ltd.
doi:10.1016/j.jsv.2005.08.009

Nomenclature

A_2 non-dimensional constant
a_j position of fluid particle prior to undergoing distortion in tensor form
b half-chord, $c/2$ (m)
c airfoil chord (m)
f frequency $\omega/2\pi$ (Hz)
G_{LL} power spectral density of lift such that $\overline{L^2}(\alpha) = \int_0^\infty G_{LL}(\alpha,\omega)\,\mathrm{d}\omega$, ($\mathrm{Pa^2/m^2\,Hz^2}$)
G^*_{LL} normalized lift spectrum, $\frac{G_{LL}(\alpha,f)}{\overline{L}^2(\alpha)}$ ($\mathrm{Hz^{-2}}$)
i $\sqrt{-1}$ or, if subscripted, tensor notation index corresponding to 1, 2, 3
k_e characteristic wavenumber, $\frac{\sqrt{\pi}}{\lambda}\frac{\Gamma\left(\frac{5}{6}\right)}{\Gamma\left(\frac{1}{3}\right)}$ ($\mathrm{m^{-1}}$)
$\hat{K}_x$ normalized wavenumber, $\frac{\omega/U}{k_e}$
k_x, k_y, k_z wavenumber vector components in the x-, y-, z-direction ($\mathrm{m^{-1}}$)
L mean lift per unit span (N/m)
L_c chordwise pressure correlation length scale, $\int_0^{x_{\max}} \frac{S_{qq}(x_i,x_j,\eta=0,f)}{S_{qq}(x_i,x_i,\eta=0,f)}\,\mathrm{d}x_j$ (m)
L_t normalized spanwise correlation length scale of inflow turbulence $\frac{8\lambda}{3}\left[\frac{\Gamma(1/3)}{\Gamma(5/6)}\right]^2 \frac{\hat{K}_x^2}{(3+8\hat{K}_x^2)\sqrt{1+\hat{K}_x^2}}$
L_η spanwise pressure correlation length scale, $\int_0^{\eta_{\max}} \frac{S_{qq}(x_i,x_j,\eta,f)}{S_{qq}(x_i,x_i,\eta=0,f)}\,\mathrm{d}\eta$ (m)
q free-stream dynamic pressure, $1/2\rho U_\infty^2$ (Pa)
r cylinder radius (m)
Re Reynolds number based on airfoil chord, $U_\infty c/\nu$
s, n curvilinear coordinate system with s directed along a streamline and n perpendicular
S_{ij} distortion tensor
S_{qq} cross-spectral density of surface pressure fluctuations ($\mathrm{Pa^2/Hz}$)
S^{Δ}_{qq} cross-spectral density of pressure difference fluctuations ($\mathrm{Pa^2/Hz}$)
t time (sec)
u', v', w' fluctuating velocity components in x-, y-, and z-direction (m/s)
$\vec{U}_\infty$ mean free-stream inflow velocity vector (m/s)
U_∞ mean free-stream velocity in x-direction (m/s)
X_1 $\frac{X_1}{U_\infty} = \frac{x_1}{U_\infty} + \int_{-\infty}^{x_1}\left[\frac{1}{U'(x_1,X_3)} - \frac{1}{U_\infty}\right]\mathrm{d}x_1$
X_3 proportional to stream-function
Φ_{ij} non-dimensional undistorted turbulence energy spectrum
$\Phi^*_{ij-\mathrm{dist}}$ non-dimensional distorted turbulence energy spectrum
$\Gamma(\,)$ gamma function
Ω_i vorticity vector ($\mathrm{s^{-1}}$)
α angle of attack (deg)
δ_{ij} Kronecker delta, 0 if $i \neq j$, 1 if $i = j$
η spanwise separation between two points, $y-y'$ (m)
λ integral scale of turbulence (m)
ν kinematic viscosity ($\mathrm{m^2/s}$)
π $\sim$3.14
ρ density ($\mathrm{kg/m^3}$)
ω angular frequency (rad/s)
ω_r reduced frequency, $2\pi fb/U$
χ_l non-dimensional distorted wavenumber vector, $k_i(S_{li})^{-1}$

The objective of this study is to provide this missing data with particular attention paid to effects of angle of attack on the airfoil response. To this end, measurements have been performed using an array of microphones embedded in the surface of a NACA 0015 airfoil placed at varying angles of attack in homogeneous turbulent flow. This work is presented in two papers; Part 1 [1] presents analysis of unsteady pressure measurements with the goal of determining the effects of mean loading. This paper discusses sources of observed mean loading effects and presents a possible model for prediction of these effects. Together, this two part series summarizes work presented by Mish [2].

2. Brief review of experiment and results

The surface pressure was measured on a 0.610 m chord NACA 0015 airfoil immersed in grid generated turbulence with an array of pressure sensors mounted subsurface. These measurements were made over a range of angles of attack, $\alpha = 0$–20°, at a mean flow velocity of 30 m/s ($Re = 1.17 \times 10^6$) with inflow

turbulence length scale, $\lambda/c = 13\%$, and turbulence intensity, $u'/U_\infty = 3.9\%$. The Virginia Tech Stability Wind Tunnel, which has a $1.83\,\mathrm{m} \times 1.83\,\mathrm{m} \times 7.32\,\mathrm{m}$ test-section, was used for this test. Further details on the experimental setup can be found in Mish and Devenport [1] and Mish [2].

Measured pressure spectral levels show a reduction of up to 5 dB with increasing angle of attack for reduced frequencies less than 5 at chordwise stations $x/c = 2.5$–14%. This observed mean loading effect has never before been measured or shown theoretically. For reduced frequencies greater than 5 a significant increase in spectral level is observed. Lift spectra, presented in Fig. 18 of Ref. [1], are used to summarize the observed effects of mean loading on the airfoil response. Lift spectra are formed by integrating pressure measurements along the airfoil chord and therefore inherently contain surface pressure and pressure difference auto- and cross-spectra. Validation of the unsteady lift formulation is presented in Mish and Devenport [1]. As shown in Fig. 18 of Ref. [1], a reduction in lift spectral level of up to 5 dB occurs for $\omega_r < 5$ as α is increased while an amplification of spectral levels occurs for $\omega_r > 5$. Again, such results have not been shown before either experimentally or theoretically.

3. Origin of low-frequency mean-loading effect

Unsteady pressure data is further examined to assist in determining where key assumptions in airfoil response theory are not valid. One particularly illuminating result shown in Part 1 (Fig. 9 of Ref. [1]) was the root mean square (rms) pressure's lack of dependence on angle of attack up to $\alpha = 14^\circ$. Such a result implies that lift spectral levels can reduce only if the correlated area over which the pressure acts is reduced. Recalling that the calculation of lift spectra in Ref. [1] was two-dimensional (lift per unit span), a reduction in correlated area implies a reduction in streamwise pressure correlation length scale. As such, an investigation into the chordwise correlation length scale is presented to offer clues about how the pressure correlation area changes with angle of attack. Furthermore, the spanwise correlation length scale is examined to assist in understanding how the inflow distorts around the leading edge of the airfoil.

3.1. Chordwise correlation length scale

3.1.1. Effects of angle of attack

The chordwise correlation length scale is presented in Fig. 1 and calculated at $x/c = 2.5\%$ for $\alpha = 0^\circ$, 4°, 8°, 12°, 16° and 20° as

$$L_c = \int_0^{x_{\max}} \frac{S_{qq}(x, x', \eta = 0, f)}{S_{qq}(x, x, \eta = 0, f)}\, \mathrm{d}x', \tag{1}$$

with L_c normalized on the airfoil chord, $x = x'$, $x_{\max} = 85\%$ chord, and S_{qq} is the *pressure difference* cross-spectral density. It is interesting to see that a reduction in L_c occurs for $\omega_r < 10$ as the angle of attack increases. The reduction in this frequency range is up to 5% of the airfoil chord and may result from the distortion of the inflow in the leading-edge region. Furthermore, the reduction in L_c with increasing α implies a reduction in the pressure correlated area (per unit span) which may be the explanation for the reduction in lift spectral level. At higher frequencies ($\omega_r > 10$) L_c reduces for small angles of attack ($\alpha < 12^\circ$) and then begins to show little variation with increasing α. The angle of attack effect revealed in L_c over this frequency range may be related to the boundary layer. High-frequency boundary layer pressure fluctuations that correlate over very small distances may be driving up the denominator of Eq. (1) (i.e. the auto-spectrum at 2.5% chord). Very little boundary layer contamination is shown in the pressure spectrum at 2.5% chord for $\alpha = 0^\circ$; however, as the angle of attack is increased and the stagnation point moves away from the suction side 2.5% chord measurement location, it is possible that boundary layer pressure fluctuations begin to become significant at high frequencies. When $\alpha = 20^\circ$ L_c rises up significantly since the airfoil is stalled and large-scale pressure fluctuations develop at low frequencies.

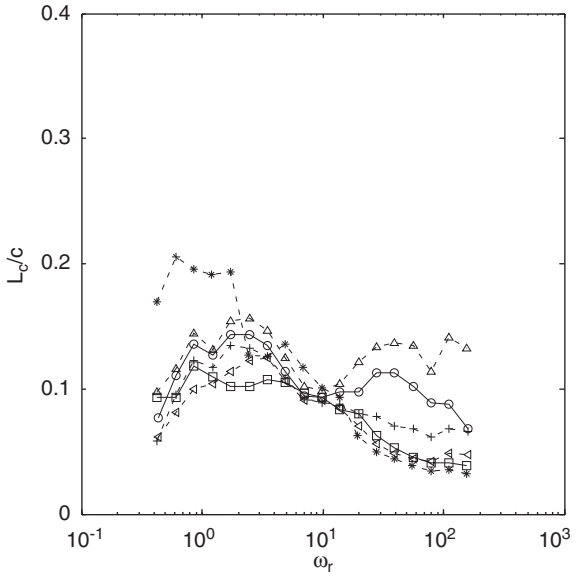

Fig. 1. Effects of angle of attack on chordwise pressure correlation length scale, L_c at $x/c = 2.5\%$ (- △- , $\alpha = 0°$; —○—, $\alpha = 4°$; - +- , $\alpha = 8°$; - ◁- , $\alpha = 12°$; —□—, $\alpha = 16°$; —✳—, $\alpha = 20°$).

3.2. Spanwise correlation length scale

The spanwise correlation length scale is computed at the five most leading-edge measurement locations ($x/c = 1\%$, 2.5%, 4%, 6%, 9%) from the pressure difference cross-spectrum as

$$L_\eta = \int_0^{\eta_{\max}} \frac{S_{qq}(x, x', \eta, f)}{S_{qq}(x, x', \eta = 0, f)}\, \mathrm{d}\eta, \tag{2}$$

where L_η is normalized on the airfoil chord, $\eta_{\max} = 96\%$ chord, and S_{qq} is the *pressure difference* cross-spectral density. This calculation is carried out at each chordwise location from 1% to 9% chord with $x = x'$ for all frequency.

3.2.1. Zero angle of attack

Fig. 2 presents L_η calculated from measured unsteady pressure as a function of frequency at $x/c = 1\%$, 2.5%, 4%, and 6% for $\alpha = 0°$ (*note*: high-frequency data was only taken in spanwise rows at 1% and 2.5% chord). The spanwise correlation length of the inflow turbulence is also presented and calculated from the von Karman spectrum [3] as

$$L_t(f) = \frac{8\lambda}{3}\left[\frac{\Gamma(1/3)}{\Gamma(5/6)}\right]^2 \frac{\hat{K}_x^2}{(3 + 8\hat{K}_x^2)\sqrt{1 + \hat{K}_x^2}}, \tag{3}$$

where

$$\hat{K}_x = \frac{\omega/U}{k_e} \quad \text{with} \quad k_e = \frac{\sqrt{\pi}}{\lambda}\frac{\Gamma(5/6)}{\Gamma(1/3)}.$$

The turbulence lengthscale L_t and the measured L_η are most consistent at 1% chord for $10 < \omega_r < 30$. This result seems logical since the surface pressure length scale in the leading edge arises from the turbulence–airfoil leading-edge interaction. Moving downstream from the leading edge, the measured L_η is shown to increase over the entire frequency range. Bearing in mind that the change in lift occurs through propagation of compressible waves with spherical wave-fronts this result seems to make good physical sense.

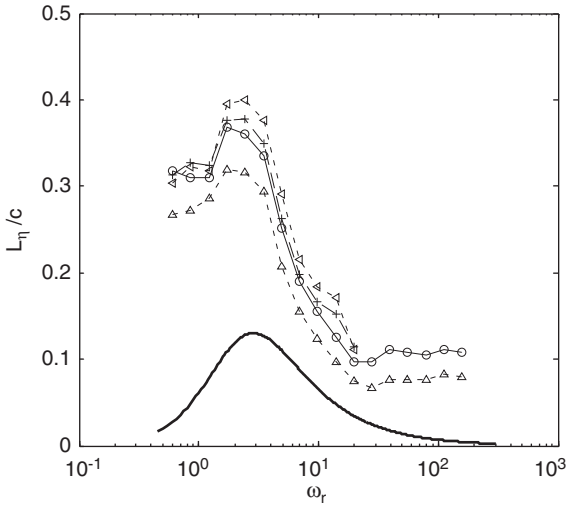

Fig. 2. Comparison of spanwise pressure correlation length scale, L_η at various chordwise stations for $\alpha = 0^\circ$ (- △- , $x/c = 1\%$; —○—, $x/c = 2.5\%$; - +- , $x/c = 4\%$; - ◁- , $x/c = 6\%$). Plotted with the spanwise length scale of the inflow turbulence computed based on Amiet (—, L_t).

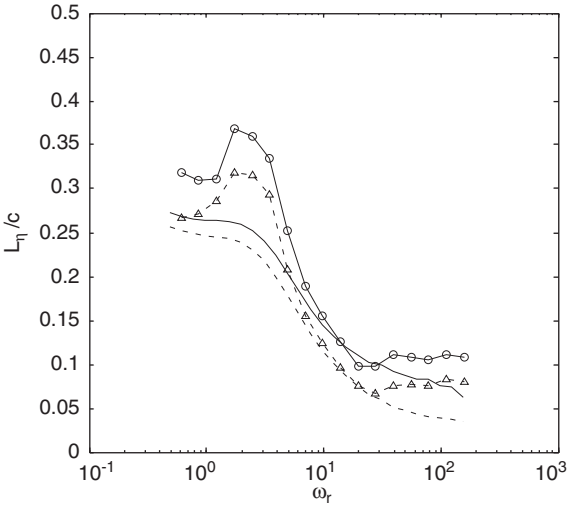

Fig. 3. Comparison of measured (- △- , $x/c = 1\%$; —○—, $x/c = 2.5\%$) and predicted (- - -, $x/c = 1\%$; —, $x/c = 2.5\%$) spanwise pressure correlation length scales, L_η for $\alpha = 0^\circ$.

Fig. 3 presents comparisons of $\alpha = 0^\circ$ measured L_η with Amiet's [4,5] predicted L_η for $x/c = 1\%$ and 2.5% chord. Amiet's theory underpredicts the spanwise length scale below $\omega_r = 10$ for all chordwise positions which is likely related to the flat-plate model used in this theory. At 1% and 2.5% chord agreement within 2% chord is shown to occur for $\omega_r > 20$. At these higher-frequencies boundary layer pressure fluctuations (high frequency), which correlate over very small spanwise separations (<1% chord) begin to contaminate L_η by driving up S_{qq} at $\eta = 0$ and thus, causing L_η to fall.

3.2.2. *Effects of angle of attack*

The variation of L_η with angle of attack is now examined in Fig. 4(a)–(d) which presents the spanwise correlation length scale as a function of reduced frequency for each angle of attack ($\alpha = 0^\circ$, 4°, 8°, 12°, 16°,

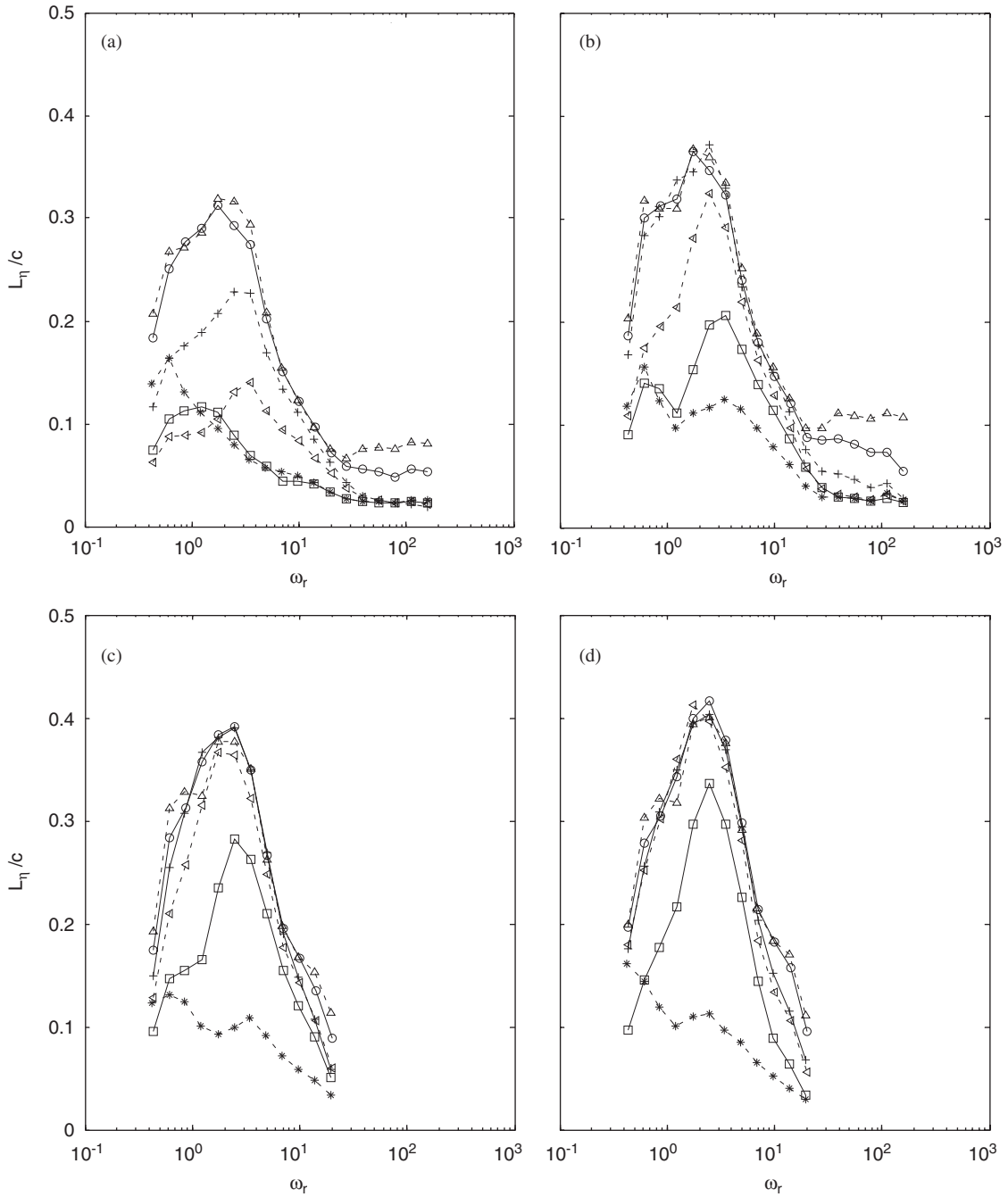

Fig. 4. Effects of angle of attack on spanwise pressure correlation length scale, L_η, at $x/c =$ (a) 1, (b) 2.5, (c) 4, and (d) 6% (– △– , $\alpha = 0^\circ$; —○—, $\alpha = 4^\circ$; – +– , $\alpha = 8^\circ$; – ◁– , $\alpha = 12^\circ$; —□—, $\alpha = 16^\circ$; —✳—, $\alpha = 20^\circ$).

20°) at $x/c = 1$, 2.5, 4, and 6% chord. At 1% and 2.5% chord locations a strong dependence on angle of attack is shown in L_η. As the angle of attack is increased L_η falls over much of the frequency range; however, most dramatically over $\omega_r < 10$. Less variation with angle of attack is shown at 4% and 6% chord for $\alpha < 12^\circ$. The airfoil is stalled at $\alpha = 20^\circ$ which seems to further drive down the extent of spanwise correlation.

3.3. Distortion of the inflow

The reduction in the spanwise and chordwise pressure correlation length scales with increasing angle of attack suggests that eddies are being increasingly stretched by the mean field producing turbulence with a smaller streamwise and spanwise length scale. This finding is contrary to the assumption made by Ref. [6] wherein the spanwise velocity correlation length was assumed to be unaffected by the distortion. Furthermore, this type of phenomenon may be the mechanism producing the reduction in unsteady loading at low reduced frequencies. Fig. 5(a) and (b) depicts how such a process could reduce the unsteady loading. At small α's the inflow eddy (labeled 'A') is convected towards the leading edge of the airfoil and moderately stretched by the mean field velocity gradients as shown in Fig. 5(a). At a higher angle of attack, the same eddy 'A' is stretched considerably more as a consequence of the increased rate of strain in the mean field which in turn reduces the eddies cross-sectional area as shown in Fig. 5(b). The eddy stretching that takes place as α increases results in a reduction in surface pressure correlation length scales (spanwise and chordwise). The reduction in L_c implies that the pressure has less of a correlated area to act over. Since the intensity of pressure fluctuations appears to remain largely unaffected by angle of attack (as shown in Part 1 [1]), the overall unsteady loading decreases with increasing angle of attack as a consequence of the reduction in correlated area.

When these results are considered in light of previous experimental work in this area (i.e. Ref. [7]), another interesting point is revealed. The distortion of the inflow appears to be critical in this experiment, wherein the integral scale (λ/c) is 13% of the chord; however, this effect does not seem to be significant in large integral scale (relative to the chord) flow such as McKeough's. Recall McKeough's measurement of unsteady lift on a NACA 0015 which showed a 3 dB (for $\omega_r < 1$) increase in lift with an increase from $\alpha = 0^\circ$ to 10° and had an inflow integral scale of 40% of the chord. The results of these two experiments suggest the relative scale of the inflow to chord length is important in determining the airfoils response when subject to mean loading. Physically this seems sensible considering that the mean field of an airfoil will not produce significant relative changes in eddies which are large compared to the airfoil. Unsteady loading models like those developed by Graham [8], Atassi [9], and Reba and Kerschen [10] seem to encapsulate mean loading effects well for this

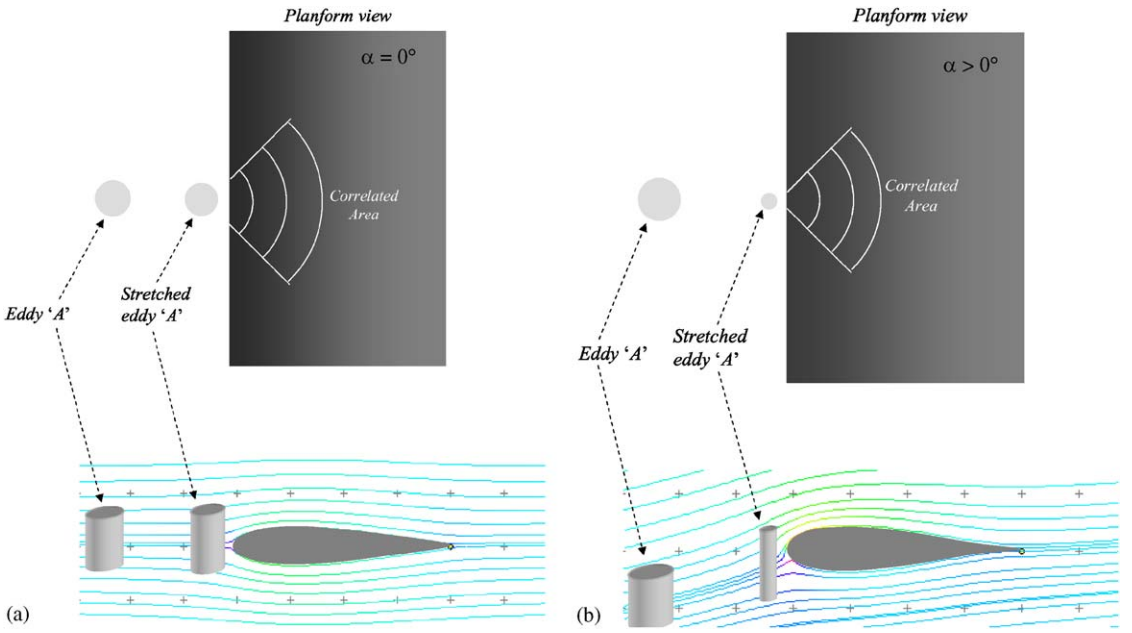

Fig. 5. Plan-form (top) and side view (bottom) of airfoil at (a) $\alpha = 0^\circ$ showing how the mean potential field moderately stretches eddy 'A' as it approaches the airfoil leading edge, and (b) at $\alpha < 0^\circ$ showing how the mean potential field *significantly* stretches eddy 'A' as it approaches the airfoil leading edge. The resulting reduction in cross-sectional area produces a reduction in the surface pressure chordwise and spanwise correlation length scale.

large-scale turbulence case. In fact, Graham's [8] theory agrees well with McKeough's [7] unsteady lift measurements based on comparisons he presented. However, for the case of small-scale turbulence (relative to the airfoil chord), Reba and Kerschen's [10] model does not depict the dominant physics of turbulence–airfoil interaction well.

4. A possible model for predicting mean-loading effects at low frequencies

In Part 1 [1] of this study, experimental data was compared with Reba and Kerschen's [10] flat-plate unsteady response theory which accounts for mean loading using Rapid Distortion Theory (RDT). RDT is a useful tool for predicting the evolution of turbulence passing through a varying rate of strain field. These comparisons revealed inadequacies in the flat-plate RDT formulation for the given λ/c in this experiment. Reba and Kerschen's theory predicted a large increase in lift spectral level with increasing angle of attack which is contrary to the measured mean loading effect. The deficiencies in this theory appear to be related to the flat-plate model assumed rather than the RDT formulation used. In fact, as revealed by the investigation of L_c and L_η above, the distortion appears to be decisive in determining the airfoil response. The trouble seems to lie in the potential field around a flat plate with leading-edge stagnation point which is sufficiently and critically different from an actual airfoil with thickness. The difference in mean fields produces incorrect predictions of turbulence evolution and thus airfoil response. Therefore, in this section, a model is presented that accurately captures the distortion of the inflow and correctly predicts mean loading effects on the airfoil response. This model use RDT to predict the distorted turbulence energy spectrum in the leading-edge region of the airfoil. The distorted energy spectrum is then used with Amiet's [4,5] flat-plate theory to predict the airfoil response.

4.1. Rapid Distortion Theory background

RDT is a scheme for predicting the evolution of turbulence as it is stretched and compressed by the mean velocity field. The foundation for this theory was laid by Batchelor and Proudman [11] and uses the linearized form of the vorticity transport equation to predict distortion effects. This theory works under the assumption that (1) distorting effects of turbulence on itself are negligible, (2) the scale of the turbulence is small compared to the scale of the distortion, and (3) the time needed for the turbulence to pass through the distortion is small, so that the influence of viscous dissipation can be neglected.

In Lagrangian form the vorticity transport equation, or what is often referred to as Cauchy's equation is given as (in tensor notation)

$$\Omega_i = \frac{\partial x_i}{\partial a_j}\Omega'_j, \tag{4}$$

where Ω'_j is the vorticity at the beginning of the distortion (time t') with position determined by a_j and Ω_i is the vorticity at the end of the distortion (time t) with position x_j. The term $\partial x_i/\partial a_j$ is referred to as the distortion tensor and will depend on the mean velocity field. Batchelor and Proudman [11] define the distortion tensor as

$$S_{ij} = \frac{\partial x_i}{\partial a_j} = \delta_{ij} + \int_{t'}^{t} \frac{\partial U_i}{\partial a_j}\,\mathrm{d}t, \tag{5}$$

where a_j is the initial position of the particle at time t', x_i is the position at time t, U_i is the mean velocity component and δ_{ij} is the Kronecker delta. Using Goldstein's [12] model the distortion tensor can be computed from a two-dimensional mean velocity field as

$$S_{ij} = \begin{bmatrix} \dfrac{\partial X_1}{\partial s} & 0 & \dfrac{\partial X_1}{\partial n} \\ 0 & 1 & 0 \\ \dfrac{\partial X_3}{\partial s} & 0 & \dfrac{\partial X_3}{\partial n} \end{bmatrix}^{-1}. \tag{6}$$

Note that in Eq. (6), the mean field does not vary in the y-direction (i.e. along the span of the airfoil) and hence the zero and unity terms. In this equation s and n form a curvilinear coordinate system with s along a streamline and n perpendicular to the streamline. The quantity X_3 is proportional to the stream function with X_1 defined as the drift function and given as

$$\frac{X_1}{U_\infty} = \frac{x_1}{U_\infty} + \int_{-\infty}^{x_1} \left[\frac{1}{U'(x_1, X_3)} - \frac{1}{U_\infty} \right] \mathrm{d}x_1, \tag{7}$$

where U' is the mean velocity component parallel to the free-stream velocity (U_∞) and x_1 is the component of the fluid particle position vector parallel to U_∞. Through manipulation of the drift function, the distortion simplifies to

$$S_{ij} = \begin{bmatrix} \dfrac{\left|\vec{U}\right|}{U_\infty} & 0 & \dfrac{\partial X_1}{\partial n} \\ 0 & 1 & 0 \\ 0 & 0 & \dfrac{U_\infty}{\left|\vec{U}\right|} \end{bmatrix}^{-1}, \tag{8}$$

where $\left|\overrightarrow{U_\infty}\right|$ is the magnitude of the mean velocity vector. The term $\partial X_1/\partial n$ is difficult to compute because it implies integration along a streamline (Eq. (7)) followed by differentiation perpendicular to the streamline; however, this calculation is feasible with careful application of numerical procedures.

Batchelor and Proudman [11] show that the distorted turbulence energy spectrum can be calculated using the distortion tensor and the undistorted energy spectrum as

$$\Phi^*_{ij-\mathrm{dist}}(\chi)\,\mathrm{d}\chi = \varepsilon_{ikl}\varepsilon_{mnp}\varepsilon_{jab}\varepsilon_{uwl}\chi_l\chi_b\chi^{-4}k_n k_u S_{km} S_{au}\Phi_{pw}(k)\,\mathrm{d}k, \tag{9}$$

where $\chi_l = k_i(S_{li})^{-1}$ is the non-dimensional distorted wavenumber vector, S_{ij} is the distortion tensor, ε_{ijk} is the unit alternating tensor and $\Phi_{ij}(k)$ is the non-dimensional undistorted energy spectrum tensor.

4.2. Airfoil response model feasibility study

A prospective unsteady response model is developed that uses a circular cylinder to predict the inflow distortion. Ideally, the distortion tensor is calculated based on the actual mean field produced by the airfoil; however, using a cylinder has the distinct advantage of significantly simplifying the distortion tensor calculation. Furthermore, much of the important inflow distortion seems to occur near the leading edge, where the radius of curvature at the stagnation point essentially defines the leading-edge geometry. As such, the distortion experienced by turbulence in this region can be approximated by fitting a circular cylinder to the airfoil at the location of the mean stagnation point. This is done at each angle of attack thereby accounting for the change in mean field as the angle of attack is varied. Fig. 6 shows a circular cylinder fit to the NACA 0015 at a location that corresponds to the $\alpha = 4^\circ$ stagnation point. The location of the mean stagnation point is readily calculated using a vortex panel method.

The stagnation streamline associated with this circular cylinder is then used to predict the distortion of the inflow via RDT (Eq. (9)) as depicted in Fig. 7. The first step in this calculation is determining the stagnation streamline velocity which is obtained for a circular cylinder from potential flow theory as

$$\frac{U(x)}{U_\infty} = 1 - \left(\frac{r}{x}\right)^2, \tag{10}$$

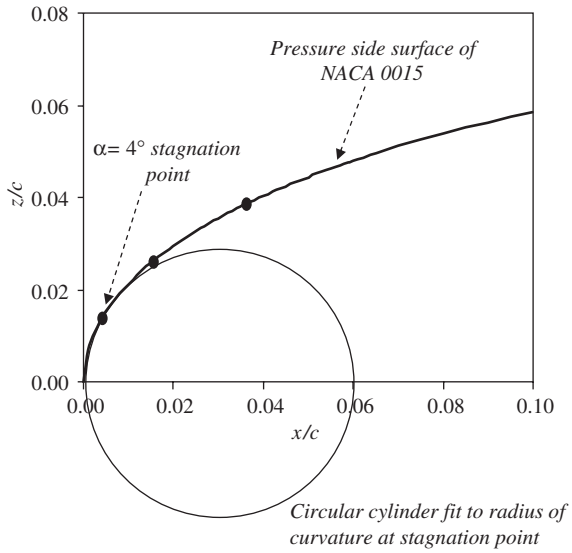

Fig. 6. Diagram showing a circular cylinder fit to the airfoils radius of curvature at the $\alpha = 4^\circ$ stagnation point location.

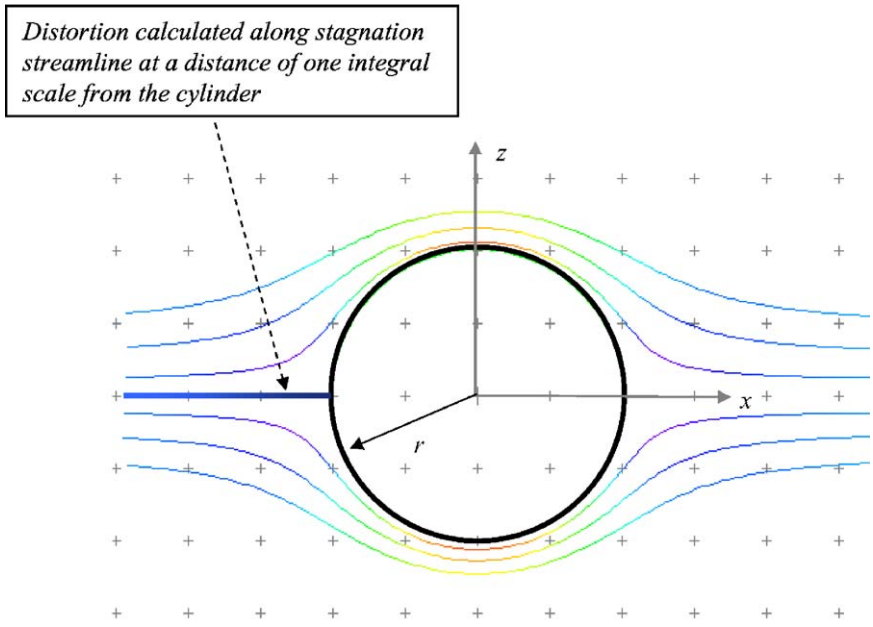

Fig. 7. Diagram showing the streamline along which the turbulence distortion is calculated.

where r is the cylinder radius. The distortion tensor is then readily computed from the potential flow solution using Eq. (8)

$$S_{ij} = \begin{bmatrix} \dfrac{U(x)}{U_\infty} & 0 & 0 \\ 0 & 1 & 0 \\ 0 & 0 & \dfrac{U_\infty}{U(x)} \end{bmatrix}^{-1}. \tag{11}$$

Notice that the most difficult term to compute in the distortion tensor, $\partial X_1/\partial n$, is zero when calculated along the stagnation streamline of a circular cylinder and hence, the real convenience of using the cylinder approximation.

This calculation is carried out for $\alpha = 0^\circ$, 4°, 8°, and 12°. The distortion is compute at a location x (referring to the notation of Fig. 7) that is some percentage of the integral scale ($\lambda/c = 13\%$) upstream of the cylinder such that

$$x = r + A_2\lambda. \tag{12}$$

The constant, A_2, is taken as 1 resulting in calculation of the distorted turbulence spectrum one integral scale upstream from the circular cylinder. The ratio of distortion location, x to cylinder radius, r for each angle of attack is given in Table 1. With the distorted turbulence spectrum computed, Amiet's [4,5] theory is used to predict the airfoil's response to the distorted inflow at each simulated angle of attack.

Table 1
Ratio of distortion location to cylinder radius

Angle of attack	x/r
0°	−9.81
4°	−3.14
8°	−2.11
12°	−1.71

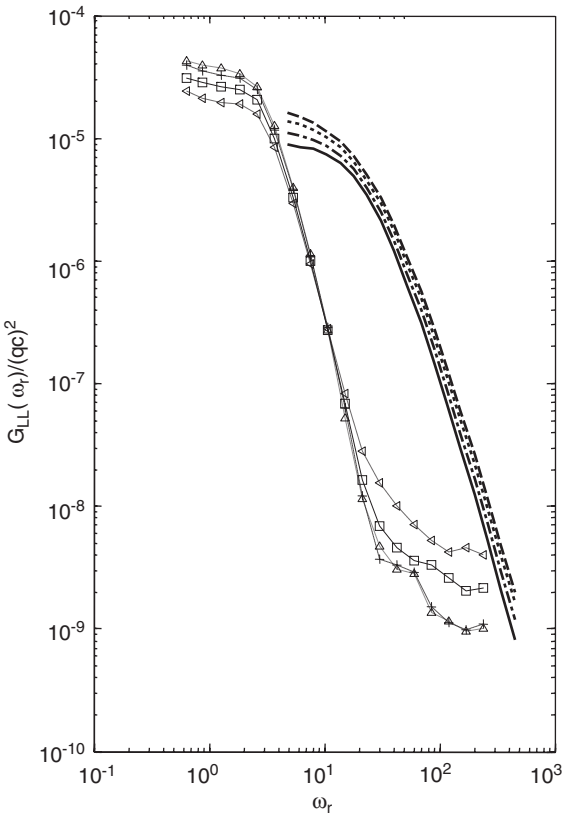

Fig. 8. Lift spectra calculated using the distorted inflow turbulence energy spectra with Amiet's solution (– △– , $\alpha = 0^\circ$; –+–, $\alpha = 4^\circ$; —□—, $\alpha = 8^\circ$; – ◁– , $\alpha = 12^\circ$) compared with lift spectra calculated from pressure measurements (- - -, $\alpha = 0^\circ$; – – –, $\alpha = 4^\circ$; — –, $\alpha = 8^\circ$; —, $\alpha = 12^\circ$). Prediction frequency is multiplied by 10 for clarity.

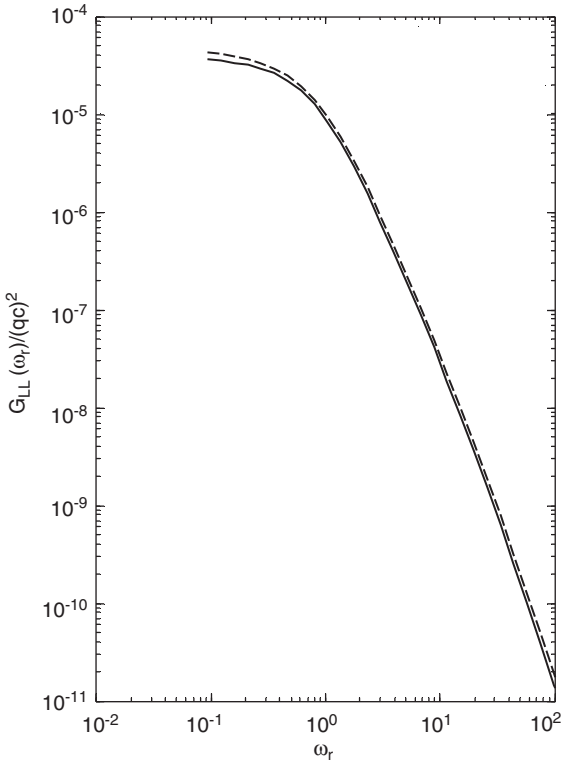

Fig. 9. Lift spectra calculated using the distorted inflow turbulence energy spectra with Amiet's solution for McKeough's flow conditions (- - -, $\alpha = 0^\circ$; —, $\alpha = 12^\circ$).

The results of this calculation are compared with lift spectra calculated from pressure measurements in Fig. 8 with normalized lift spectra, G_{LL} plotted against ω_r for $\alpha = 0^\circ$, 4°, 8°, and 12°. The model lift spectra are calculated discretely using the same six chordwise locations used to calculate lift from measured pressure. This new unsteady loading prediction scheme shows a 6 dB reduction is lift and under estimates spectral levels by not more than 5 dB for $\omega_r < 10$ as α is increased from 0° to 12°. This is excellent prediction of the angle of attack trend and surprisingly good prediction of the spectral levels in light of the approximations used in the formulation (i.e. calculation of distortion one integral scale upstream of a circular cylinder). This model also predicts some reduction in unsteady lift for $\omega_r > 10$ which is not shown in the measurement. Clearly though, this model provides evidence that, in fact, the distortion of the inflow is crucial in producing the reduction of unsteady lift with increasing angle of attack.

To shed additional light on the relative importance of the inflow distortion for large-scale turbulence (large relative to chord length), this model is used to predict the unsteady lift based on McKeough's [7] flow conditions ($U_\infty = 15\,\mathrm{m/s}$, $\lambda/c = 0.4$, $u'/U_\infty = 6.5\%$). This calculation is carried out as outlined above with $x/r = 3.1$ and 27.2 which corresponds to $\alpha = 0^\circ$ and 12°, respectively. Fig. 9 presents the predicted lift spectra as a function of ω_r. Less than 1 dB of reduction in lift spectral level is predicted for $\omega_r < 10$ with the spectra falling nearly on top of each other for higher frequencies. As expected, this theory does not predict the increase in unsteady lift shown to occur in McKeough's measurements. However, this prediction does prove the point that the inflow distortion is not an important factor in determining the unsteady loading for $\lambda/c = 40\%$ (e.g. large-scale turbulence relative to chord length) and in fact, those factors which are correctly modeled in Graham's [8] theory are likely dominant.

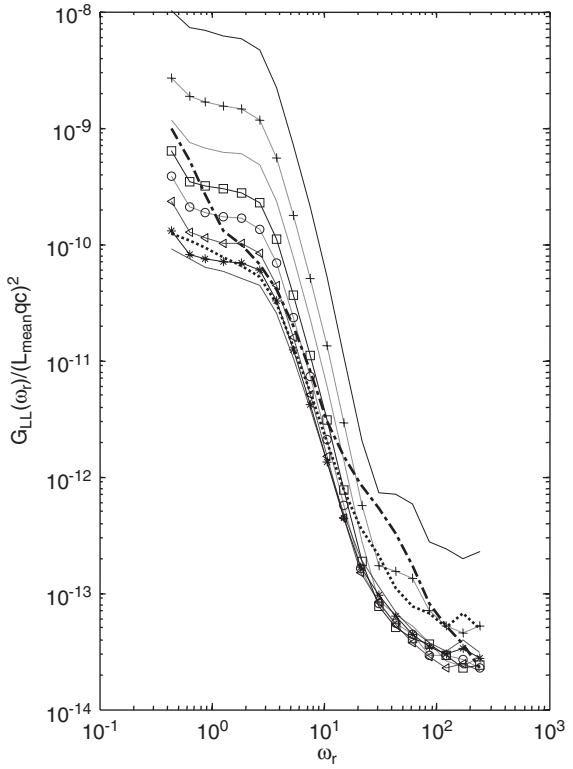

Fig. 10. Lift spectra scaled on the mean lift squared (—, $\alpha = 2°$; – + –, $\alpha = 4°$; - - - - -, $\alpha = 6°$; —□—, $\alpha = 8°$; —○—, $\alpha = 10°$; – ◁– , $\alpha = 12°$; —✳—, $\alpha = 14°$; – –, $\alpha = 16°$; - - - - - , $\alpha = 18°$; – – –, $\alpha = 20°$).

5. High-frequency angle of attack effect

Lift spectra calculated from pressure measurements (Fig. 18 of Ref. [1]) show an increase in spectral level with increasing angle of attack for $\omega_r > 10$ that can be explained by scaling lift spectra on the square of the mean lift as

$$G^*_{LL}(\alpha, f) = \frac{G_{LL}(\alpha, f)}{L^2(\alpha)}, \tag{13}$$

where G_{LL} is the unsteady lift and L^2 is the mean lift squared.

Fig. 10 presents the scaled lift spectra (note, data for $\alpha = 0°$ is not presented due to singularity which results from zero mean lift) as a function of reduced frequency. This scaling amplifies the effects of mean loading at low frequencies ($\omega_r < 10$) causing a greater reduction in lift spectral level with increasing angle of attack. However, above $\omega_r = 10$ the lift spectra collapse to within 5 dB by the mean lift scaling for $\alpha > 4°$. This is a considerable reduction in the 10 dB of variation with angle of attack shown over this frequency range in the unscaled lift spectra. The collapsing of data over this frequency range suggests the variation in unsteady lift here is closely related to the mean loading on the airfoil and in particular the mean pressure field. In this frequency range pressure fluctuations result largely from the turbulent boundary layer and free-stream eddy convection (as discussed in Ref. [1]) and consequently do not correlate from one side of the airfoil to the other. The physical explanation for this scaling may be related to thickening of the boundary layer on the suction side of the airfoil as the angle of attack increases. The suction side boundary layer grows thicker as α increases as a consequence of the increasing adverse pressure gradient. A thicker turbulent boundary layer contains larger-scale eddies that produce larger pressure fluctuations which in turn generates increased unsteadiness in the lift at high frequencies.

6. Conclusions

This paper is the second in a series of two papers (Part 1 [1] and 2) that experimentally investigates mean loading effects and their sources on the response of an airfoil encountering turbulence. Unsteady pressure measurements were made on the surface of a NACA 0015 immersed in grid turbulence ($\lambda/c = 13\%$) for angles of attack $\alpha = 0$–20°. This paper (Part 2) presents the sources of the low-frequency reduction and high-frequency increase observed in measured lift and pressure spectral levels.

The increase in lift spectral level observed for $\omega_r > 10$ appears to be related to the change in mean pressure field based on scaling lift spectra on the mean lift squared. Based on analysis of the chordwise and spanwise pressure correlation length scale, the reduction in unsteady lift at low frequency is believed to result from distortion of the inflow by the mean velocity field. However, prediction methods such as Reba and Kerschen [10] that use Rapid Distortion Theory to account for mean loading effects do not show this reduction in lift spectral level as a consequence of the flat-plate model assumed. As such, a possible model is developed that accurately predicts mean loading effects on lift spectra. This model uses a circular cylinder fit to the airfoil to compute effects of distortion on the inflow turbulence. The distorted inflow velocity spectrum is then used with Amiet's [4,5] theory to predict the unsteady loading. This model successfully captures the reduction observed in lift spectra calculated from pressure measurements. Furthermore, it is shown that angle of attack effects arising from inflow distortion are significant only when the relative scale of the inflow turbulence to airfoil chord is sufficiently small ($\lambda/c = 13\%$ for the present experiment). Factors which are well predicted by the theories such as Graham [8], Atassi [9], Reba and Kerschen [10] become dominant when the scale of the inflow is large compared to the airfoil chord.

Acknowledgments

This work would not have been possible were it not for the kind support of Casey Burley and Tom Brooks of NASA Langley under Grant NAG-1-2272. Their insight and feedback on the analysis of this substantial data set is also appreciated.

References

[1] P.F. Mish, W.J. Devenport, An experimental investigation of unsteady surface pressure on an airfoil in turbulence, Part 1: effects of mean loading, *Journal of Sound and Vibration*, 2003, under review.
[2] P.F. Mish, An Experimental Investigation of Unsteady Surface Pressure on Single and Multiple Airfoils, PhD Dissertation, Aerospace and Ocean Engineering Department, Virginia Tech, March 2003. Available at http://scholar.lib.vt.edu/theses/available/etd-03312003-173021/.
[3] R.K. Amiet, Acoustic radiation from an airfoil in a turbulent stream, *Journal of Sound and Vibration* 41 (4) (1975) 407–420.
[4] R.K. Amiet, High-frequency thin airfoil theory for subsonic flow, *AIAA Journal* 14 (8) (1976) 1076–1082.
[5] R.K. Amiet, Airfoil response to an incompressible skewed gust of small spanwise wave-number, *AIAA Journal* 14 (4) (1976) 541–542.
[6] S. Moreau, M. Roger, V. Jurdic, Effect of angle of attack and airfoil shape on turbulence-interaction noise, *11th AIAA/CEAS Aeroacoustics Conference Meeting and Exhibit*, May 23–25, 2004, Monterey, California.
[7] P.J. McKeough, Effects of Turbulence on Aerofoils at High Incidence, PhD Dissertation, University of London, 1976.
[8] J.M.R. Graham, Lifting surface theory for the problem of an arbitrarily yawed sinusoidal gust incident on a thin airfoil in incompressible flow, *Aeronautical Quarterly* (1970) 182–198.
[9] H.M. Atassi, Sears problem for a lifting airfoil revisited-new results, *Journal of Fluid Mechanics* 141 (1984) 109–122.
[10] R.A. Reba, E.J. Kerschen, Influence of airfoil angle of attack on unsteady pressure distributions due to high-frequency gust interactions, Report to NASA Langley Research Center, 1996.
[11] G.K. Batchelor, Proudman, The effects of rapid distortion on a fluid in turbulent motion, *Quarterly Journal of Mechanics and Applied Mathematics* 7 (Part 1) (1954) 83–103.
[12] M.E. Goldstein, Turbulence generated by the interaction of entropy fluctuations with non-uniform mean flows, *Journal of Fluid Mechanics* 93 (Part 2) (1979) 209–224.